

THEMALLY INDUCED SLOPE FLOWS

Xiurong Sun\*, Wensong Weng, Peter A. Taylor  
York University, Toronto, Ontario

1. INTRODUCTION

Slope wind systems are common characteristic of atmospheric boundary layer (ABL) over complex terrain. Slope winds are produced by temperature differences between air adjacent to the slope and ambient air at the same altitude outside the slope boundary layer due to diurnal surface radiative cooling and heating. Clear skies (strong solar insolation) and weak synoptic winds are conducive for the development of well-defined slope flows (Whiteman, 1990, 2000). Slope wind systems are categorized into downslope, katabatic or drainage wind, and upslope or anabatic wind. Typically, winds flow up-slope during daytime and downslope during nighttime. Slope flows may occur over very weak slopes and aggregations of these flows can also result in larger scale flows such as valley and mountain winds. These flows span a broad range of scales, from small scale of a few kilometers to mesoscale thermal circulations with horizontal scales on the order of 100km or more. They have significant effects on the transfers of heat and moisture, and the transport and dispersion of air pollutants from the boundary layer to the overlying free troposphere. The above background has motivated interest in studies of these flows in the last few decades. Recent related field campaigns include "Vertical Transport and MiXing" (VTMX) field experiment, Salt Lake City, USA, 2000 (Monti, et al., 2002) and Pacific 2001 Air Quality Field Study in the Lower Fraser Valley, British Columbia, Canada (Reuten et al., 2002), etc.

Good turbulence closure schemes are important for numerical modeling because simulations of turbulent fluxes of boundary-layer momentum, heat and mass are significantly affected by them. To investigate the vertical structure of slope flows and physical process within the slope layer, a 1D model is valuable for fine-resolution tests of turbulent closure schemes and other boundary-layer parameterizations. Six commonly used turbulence closure schemes for the ABL are applied to simulate slope flows within our simplified model in order to get the model results from the different closures which are not obscured by difference in overall the model formulation. Model simulations are also compared with observations of katabatic flows over the sloping ice surface of the Vatnajökull in Iceland, in the summer of 1996 (Oerlemans et al.1999; Van Der Avoird and Duynkerke 1999). In addition, the effects of physical parameters, such as the slope angle, surface roughness, surface cooling, and atmospheric stability on the slope winds are studied. Finally, diurnal cycles of idealized slope

winds are simulated under calm background winds and in stably-stratified ambient conditions.

2. MODEL DESCRIPTION

2.1 Mean Equations

Following the coordinate transformation ( $x = x, y = y, z^* = z - z_g(x)$ ), and for simplicity, considering an idealized, horizontally homogeneous sloping surface in the absence of radiative flux divergence and moisture, mean Navier-Stokes equations after Reynolds averaging are transformed and simplified as:

$$\frac{\partial U}{\partial t} = \frac{\partial z_g}{\partial x} \frac{\Theta}{\Theta_0} g + f(V - V_g) - \frac{\partial \overline{uw}}{\partial z^*} \quad (2.1)$$

STO= KAT      COR    LSC    TUR

$$\frac{\partial V}{\partial t} = -f(U - U_g) - \frac{\partial \overline{vw}}{\partial z^*} \quad (2.2)$$

STO= COR    LSC    TUR

$$\frac{\partial \Theta}{\partial t} = -(U - U_0) \frac{\partial \Theta_0(z)}{\partial z^*} \frac{\partial z_g}{\partial x} - \frac{\partial \overline{w\theta}}{\partial z^*} \quad (2.3)$$

STO=            VAD            TUR

Here the notation used is,

$U, V$  wind components in the x and y directions

$U_g, V_g$  geostrophic wind speed components

$f$  Coriolis force

$g$  gravitational acceleration

$\Theta_0(z)$  reference state potential temperature

$\Theta$  potential temperature perturbation from the ambient

$z_g(x)$  ground elevation

$u, v, \theta$  remaining turbulent fluctuations.

The individual terms in the above equations are named as follows:

STO	denotes	storage / tendency
KAT		katabatic forcing
TUR		turbulent diffusion
VAD		vertical advection
COR		Coriolis forcing
LSC		large-scale forcing

In the above equations, any dependent variables are partitioned into the ambient part and a perturbation associated with local cooling or heating. Synoptic scale

\* Corresponding author address: Xiurong Sun, CRESS, York University, Toronto, Ontario M3J 1P3, CANADA.  
E-mail: xrsun@yorku.ca

pressure variations are represented by the geostrophic wind. Hydrostatic equilibrium and incompressibility are assumed. The effects of molecular viscosity are neglected.

### 2.2 Descriptions of Turbulence Closure Schemes

Turbulence closure schemes considered in this study use the local gradient diffusion assumption to calculate the vertical flux of a transported quantity. They are all 1.5-order schemes in which the equations for the turbulent kinetic energy (TKE) and a turbulence length scale are used. The turbulent length scale equation can either be diagnostic ( $E-\ell$ ,  $E-\varepsilon-\ell$ , and  $q^2\ell$  - Model I) or prognostic ( $E-\varepsilon$  or its modification and  $q^2\ell$  - Model II). A detailed description of these six turbulence closure schemes is given by Weng and Taylor (2003). A summary of the main features of the schemes is provided in Table I.

Table I. List of turbulence closure schemes used in this study

Turbulence closure	Based on	Diagnostic	Prognostic
$E-\ell$	Delage (1974)	$\ell$	$E$
$q^2\ell$ Model I	Mellor and Yamada (1982)	$\ell$	$q^2$
$q^2\ell$ Model II	Mellor and Yamada (1983)	-	$q^2, q^2\ell$
$E-\varepsilon$	Standard form, Holt and Raman (1988)	-	$E, \varepsilon$
$E-\varepsilon$ (DE85)	Detterling and Etling (1985)	-	$E, \varepsilon$
$E-\varepsilon-\ell$	Xu and Taylor (1997)	$\ell$	$E, \varepsilon$

### 2.3 Numerical Schemes and Boundary Conditions

Expecting strong gradients near the surface, a log-linear coordinate is used. 141 grid points cover 3 km of ABL. Turbulent and mean quantities are placed on a staggered grid where mean velocity and temperature are placed on the intermediate grid levels and turbulent quantities are placed on grid levels. The resulting prognostic equations for momentum, heat, TKE and its dissipation rate are numerically in time. The numerical scheme used for time integration is Crank-Nicholson scheme. The system of difference equations is solved using a block LU factorization algorithm (Karpik 1988). To model cases where the surface roughness,  $z_0$ , and surface temperature scaling length are different, a wall layer is added, as recommended by Taylor and Delage (1971). The first two levels for mean variables are at about 0.09 m and 0.13 m.

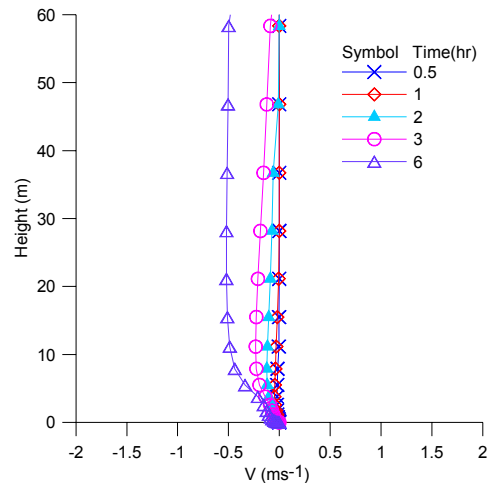
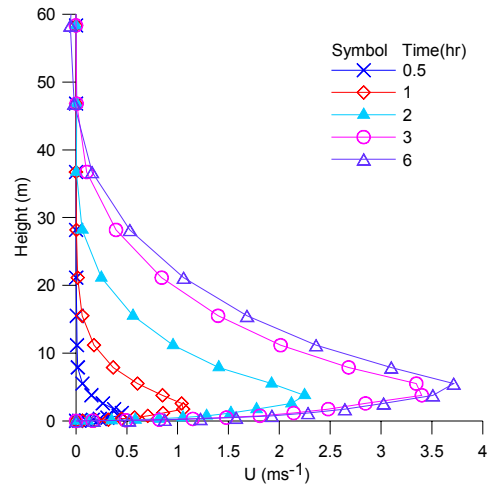
The surface boundary conditions are a non-slip condition for velocity ( $U=V=0$ ), a specified time dependent temperature or heat flux and the assumption that TKE production balances dissipation. At the upper boundary, the vertical derivation of TKE, its dissipation rate and potential temperature perturbation are zero and wind speed is equal to geostrophic wind.

For cases without ambient winds, following a procedure discussed by Rao and Snodgrass (1981), Prandtl's analytical solutions are used to specify the

approximate initial profiles. The model is numerically integrated for one inertial cycle to obtain the approximate equilibrium state, which is then used as the initial conditions. Note that this procedure ensures that the model results are independent of the approximate initial conditions. For cases with ambient winds, the initial profiles are a neutral Ekman boundary layer.

Table II. Model parameters and case conditions

Model parameter	Case 1	Vatnajokull	Sensitivity case
Surface cooling rate ( $\text{Khr}^{-1}$ )	2		2
Surface temperature deficit (K)	6	10	6
Stratification ( $\text{K km}^{-1}$ )	6	4.5	6
Slope ( $^\circ$ )	10	4.5	5
Geostrophic wind ( $U_g, V_g$ ) ( $\text{ms}^{-1}$ )	0,0	0,0	0.0
$z_i, z_0$ (m)	0.1	0.00004, 0.002	0.002
Entrainment velocity ( $\text{ms}^{-1}$ )	-	0.01	-



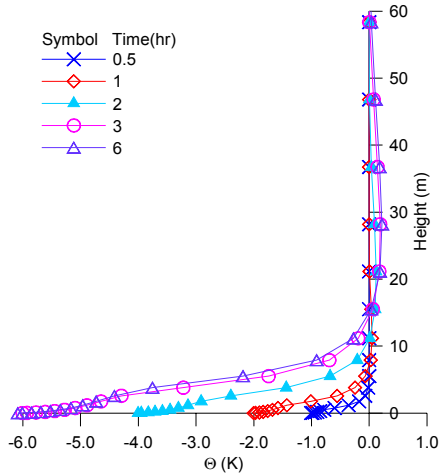


Figure 1. Predicted evolution of mean velocity and potential temperature deficit profiles by  $q^2 l$  Model I.

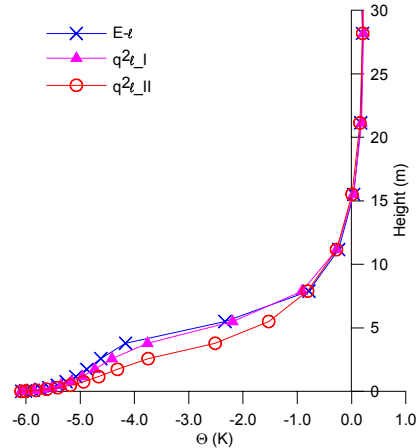
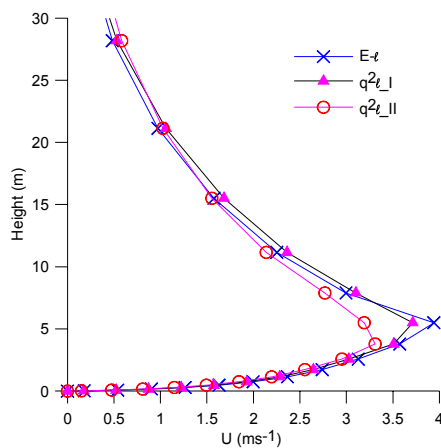
### 3. MODEL RESULTS

#### 3.1 Comparison of Different Turbulence Closure Schemes

The model is first used to simulate downslope winds in order to compare six turbulence closure schemes. The input parameters for this case condition (referred to as Case 1) are given in Table II. Figure 1 presents the predicted evolution over a 6hr period of the mean velocity and potential temperature profiles using  $q^2 l$  Model I closure. As can be seen,  $q^2 l$  Model I produces typical nighttime downslope flows, with a very shallow flow layer. It is characterized by a very stably stratified temperature structure, large wind component (U) and a prominent velocity maximum (low-level jet) near the surface in the along-slope direction (x axis). These characteristics of downslope flows are similar to simulations and observations of other studies (Rao and Snodgrass, 1981; Doran and Horst, 1983; Yamada, 1983; Denby, 1999; etc.). This can be compared with simulations of the pure downslope winds by Rao and Snodgrass, 1981. The wind speed, the downslope layer depth, the velocity maximum and jet height all increase

with the increase of surface temperature deficit. Obviously, the surface cooling contributes to development of down-slope flow. For the cross-slope direction, a small wind component (V) is produced due to the Coriolis force, which is balanced by turbulent diffusion. For simplicity, wind component U will be the study topic of interest.

Maintaining the boundary conditions and with the surface temperature deficit held at a constant value of 6K, the model is numerically integrated for a further 6 hrs to get the equilibrium state as indicated by invariant turbulent fluxes. The steady state profiles of wind and temperature and turbulent quantities using six turbulence closures are shown in Figures 2 and 3. As can be seen, the predicted mean wind and potential temperature deficit from  $E-l$  and  $q^2 l$  Model II are similar to those from  $q^2 l$  Model I with minor difference.  $E-\epsilon$  and  $E-\epsilon-DE$  model shows similar results, predicting the largest layer depth and the strongest turbulence. This is a similar conclusion to the comparison made by Weng and Taylor (2003) over flat terrain. With modifications, the  $E-\epsilon-DE$  model predicts a slightly smaller layer depth than  $E-\epsilon$  and simulations with  $E-\epsilon-l$  give the similar results of  $E-l$  and the two  $q^2 l$  models. The significant differences among  $E-l$ ,  $E-\epsilon-l$  and two  $q^2 l$  Models are wind speed maxima and temperature profiles at jet height and below jet height. The  $E-l$  model gives a slightly larger wind speed and a slightly larger temperature gradient below jet height than the  $q^2 l$  models. The “nose” in the wind profile using  $q^2 l$  is smaller than that using  $E-l$  model, which is different from the simulations by Yamada (1983) probably because the constraints of a minimum value of turbulent mixing length were chosen. Those are probably caused by different eddy diffusivities for momentum and TKE, which are significant different at and below the jet height regions, especially the eddy diffusivities for TKE.



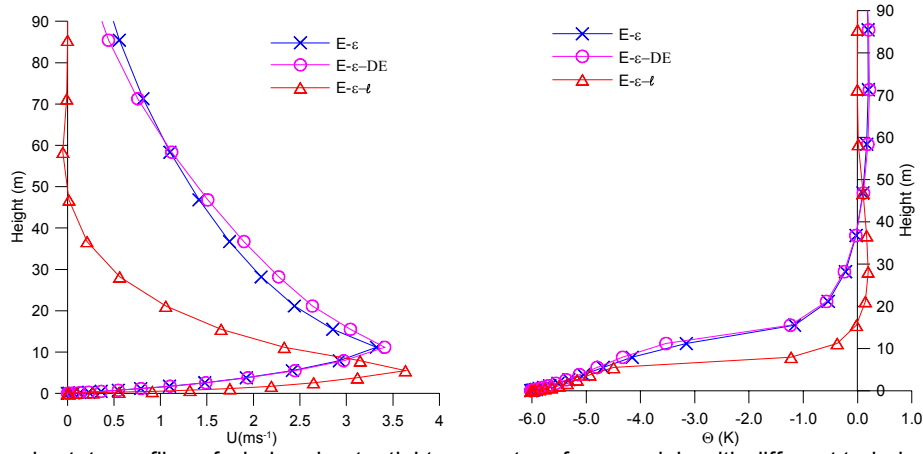


Figure 2. Steady state profiles of wind and potential temperature from models with different turbulence closures.

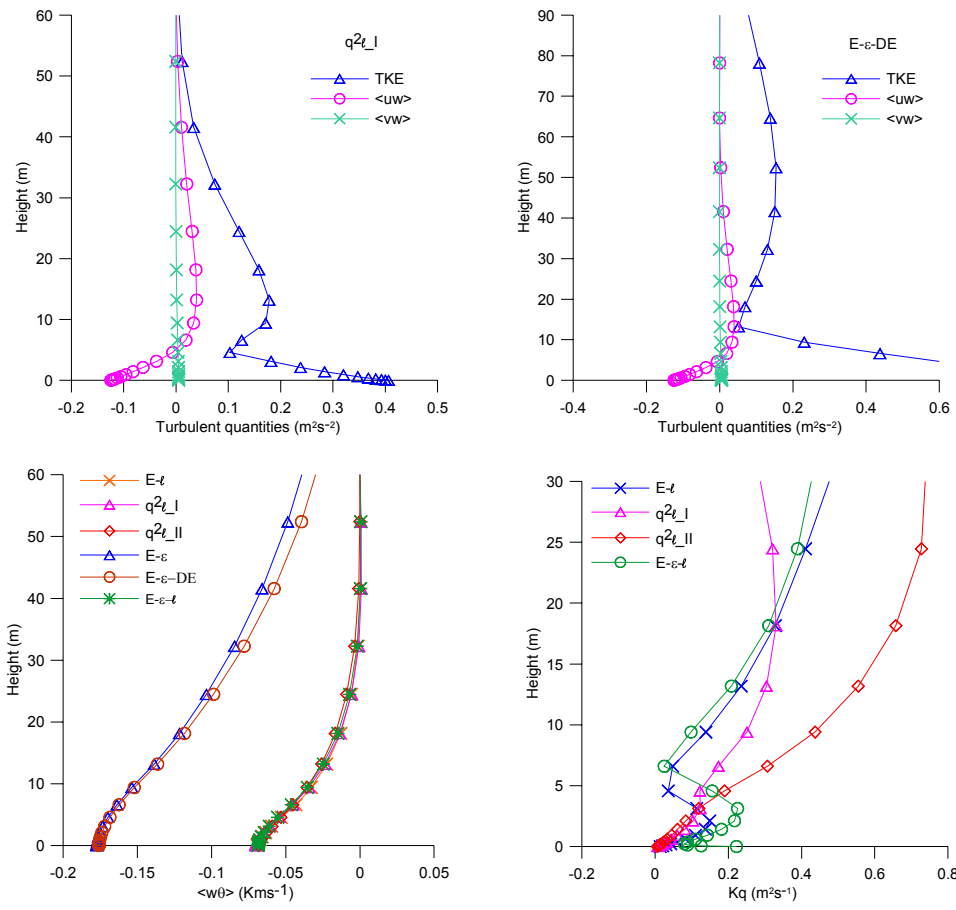


Figure 3. Profiles of turbulent quantities from  $q^2 \ell$  Model I and  $E-\varepsilon$  (DE85), and heat flux, eddy diffusivity for TKE profiles from models with different turbulence closures.

### 3.2 Comparison with Observations

It is very important to compare the model simulations with observations to examine the ability of the model to simulate katabatic winds. Based on their good performance and differences between the schemes, two turbulent schemes,  $E-\ell$  and  $q^2 \ell$  Model I are selected to simulate the katabatic flows taken over the sloping ice

surface of Vatnajökull, Iceland. The observed data are from profile mast, balloon sounding, sonic anemometer and sodar measurements. The weather condition was good for downslope winds to develop (Denby 1999). For model parameters see Table II; an entrainment velocity is also introduced into the model simulations as was done by Denby 1999 to represent the other effects

which are not taken account in a one-dimensional model. Comparisons of observed and modeled mean profiles and turbulent quantities by our  $q^2\ell$  model I are given in Figure 4. Good agreement with observations is found for both mean wind and temperature profiles as well as turbulent quantities with a slightly under-predicted TKE.

Model results from the  $E-\ell$  model show profile mast measurements and turbulent quantities are also reproduced very well but agree less well with the tethered balloon sounding data.

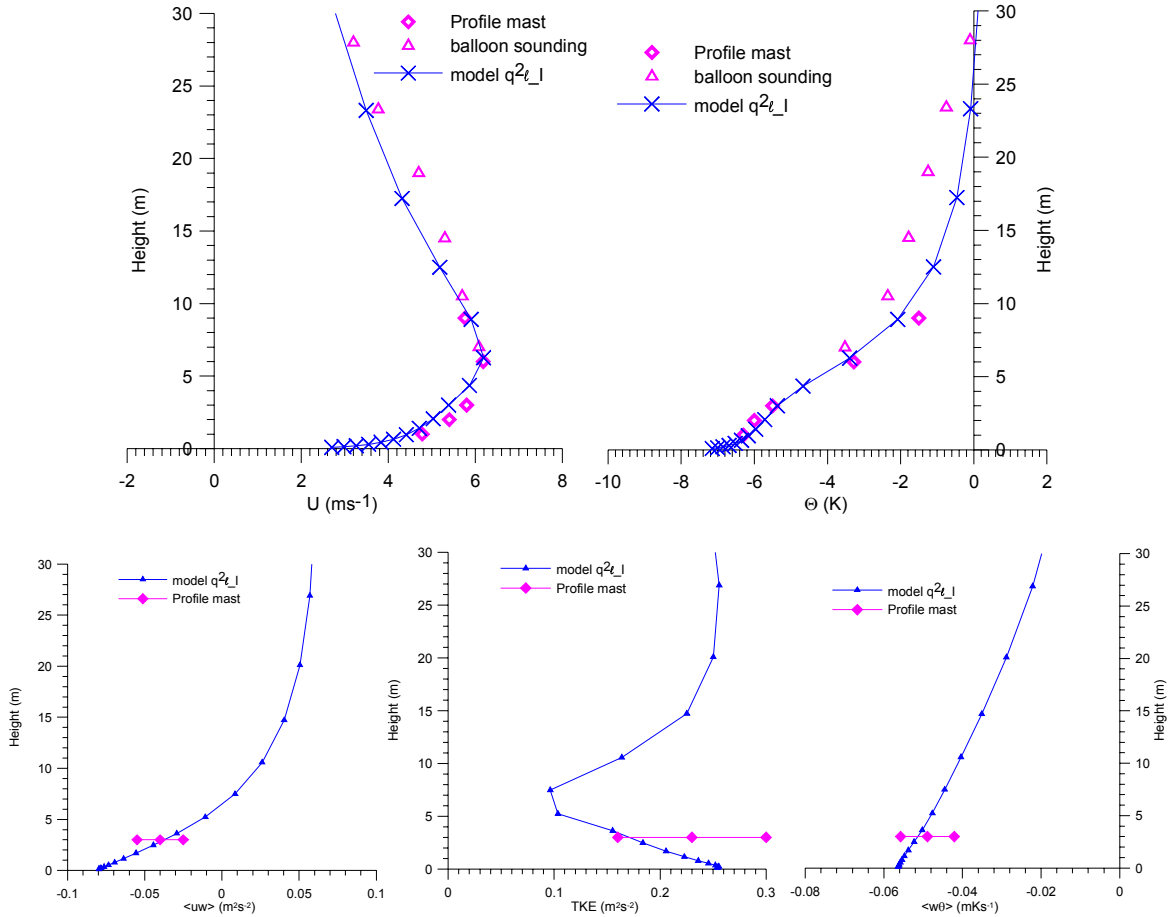


Figure 4. Comparison of modeled  $q^2\ell$  Model I and observed mean profiles and turbulent quantities. Solid lines indicate the model simulation. Squares indicate profile mast measurements; triangles represent balloon sounding measurements and diamonds with error bars, indicating the standard deviation over the observational period.

### 3.3 Sensitivity Experiments

The effects of physical parameters, such as the slope angle, surface roughness and atmospheric stabilities on the downslope winds are investigated using results from the  $q^2\ell$  Model I. Only the effects of surface roughness on slope winds are discussed here. The steady state profiles of wind and temperature with different surface roughness ( $z_0$ ) have been studied. The downslope layer, jet height and wind speed maxima decrease with the decrease of the surface roughness because not only turbulent friction forces but also katabatic forces decrease due to the decrease of the surface roughness, which is in agreement with simulations by Rao and Snodgrass (1981).

### 3.4 Diurnal Cycle of Slope Winds

The model runs are carried out for 10 days with the surface potential temperature repeating cyclically every 24 hr to produce a diurnal cycle of idealized slope winds under calm background winds and stably stratified ambient conditions. Note that the model is a one dimensional model with the greatly simplified assumptions. It is much idealized but general features from simulations are similar to the observations. Figure 5 shows the modeled diurnal cycle of slope wind with the  $q^2\ell$  Model I and  $E-\ell$  closures. As we can see, downslope or upslope wind develops with the surface cooling or heating. Profiles of the upslope winds differ significantly from those of downslope flows. The profiles of downslope flows have the obvious jet while the profiles of upslope

flows are quite uniform. The upslope layer is much deeper than downslope layer. Similar features occur in temperature profiles. The differences can be explained by turbulent fields. The air within downslope flows is very stable. Turbulence in such stable flows is suppressed, inhibiting the vertical exchange of momentum and heat, and consequently large vertical gradients of properties exist, whereas for the upslope layer, the ve-

locity and heat gradients are very small thanks to strong turbulent transports in the vertical direction. Comparison of results with  $q^2 \ell$  Model I and  $E-\ell$  closures shows that they produce quite similar nighttime downslope flows, but the  $q^2 \ell$  Model I produces a much deeper upslope layer.

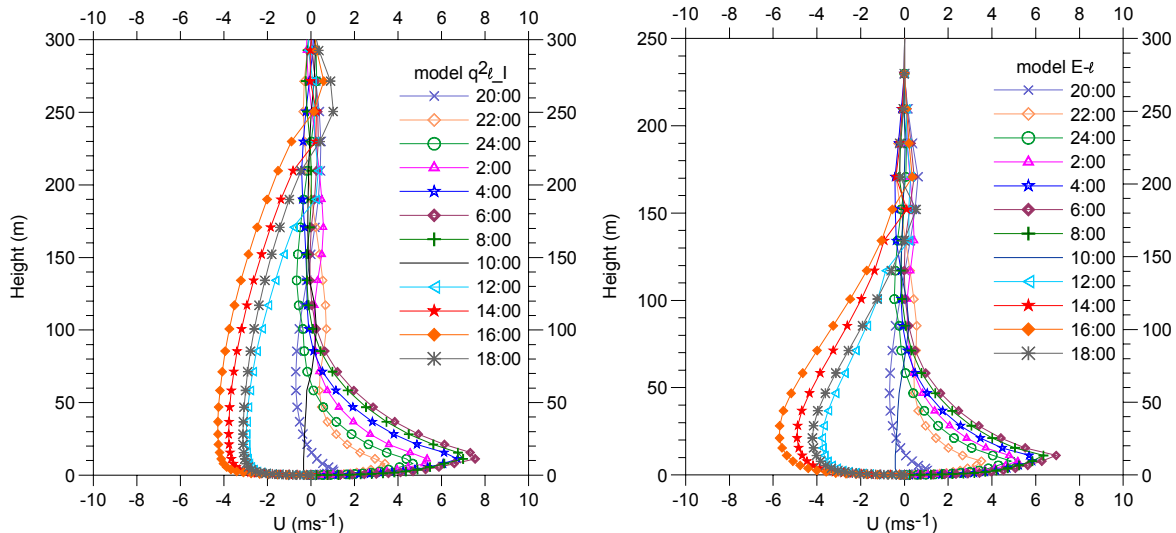


Figure 5. Modeled diurnal cycle of slope wind ( $U$ ) by  $q^2 \ell$  Model I and  $E-\ell$ .

#### 4. CONCLUSION AND DISCUSSION

A one-dimensional high-resolution ABL model for studying slope flows has been developed and improved. It is applied to significantly different case studies of slope flows, slope angles varying from small slope to steeper slope, roughness lengths from an ice surface to a rough surface. It seems it works very well. The model is used to evaluate several turbulence closure schemes to understand the effects of turbulence closures on model results in terms of simulations of downslope flows, which demonstrates appropriate differences in different schemes. Model results using  $E-\ell$  and  $q^2 \ell$  Model I are also compared with observations of katabatic flows. In general,  $q^2 \ell$  Model I performs the best of six different turbulent closure schemes.

Model results are being analyzed so some simple conclusions are given above. Extended and detailed analysis and explanations of modeling will be continued. More field data need to be compared with model results. Numerical simulations of slope flows and turbulence in these flows will be further investigated within the multi-dimensional version model, the Advanced Regional Prediction System (ARPS).

#### ACKNOWLEDGEMENTS

This research has been supported in part from the NSERC grant for MAGS2. We are grateful to Hans Oerlemans for discussions on the Vatnajokull study.

#### REFERENCES

- Businger J.A., 1973: Turbulent transfer in the atmospheric surface layer, in Haugen D.A. (ed.), Workshop on Micrometeorology, American Meteorological Society, Boston.
- Delage Y., 1974: A numerical study of the nocturnal atmospheric boundary layer. *Quart. J. Roy. Meteorol. Soc.* 100: 251–265.
- Denby B., 1999: Second-order modeling of turbulence in katabatic flows. *Boundary-Layer Meteorol.* 92: 67–100
- Detering H.W., Etling D., 1985: Application of the  $E-\epsilon$  turbulence model to the atmospheric boundary layer. *Boundary-Layer Meteorol.* 33: 113–133.
- Doran, J. C. and Horst, T. W., 1983: Observations and Models of Simple Nocturnal Slope Flows, *J. Atmos. Sci.* 40, 708–717.
- Holt T., Raman S., 1988: A review and comparative evaluation of multilevel boundary layer parameterization for first-order and turbulent kinetic energy closure schemes. *Rev. Geophys.* 26:761–779.
- Karpik S. R., 1988: An improved method for integrating the mixed spectral finite difference (MSFD) model equations. *Boundary-Layer Meteorol.* 43: 273–286.

- Mellor G.L., Yamada T., 1982: Development of a turbulence closure model for geophysical fluid problems. *Rev. Geophys. Space Phys.* 20: 851–875.
- Monti P., H.J.S. Fernando, M. Princevac, W.C. Chan, T.A. Kowalewski and E.R. Pardyjak, 2002: Observations of flow and turbulence in the nocturnal boundary layer over a slope. *J. Atmospheric Scs.* vol. 59(17), 2513-2534.
- Oerlemans J., Björnsson H., Kuhn M., Obleitner F., Palsson F., Smeets C. J. P. P., Vugts H. F., de Wolde J., 1999: Glacio-meteorological investigations on Vatnajökull, Iceland, summer 1996: an overview. *Boundary-Layer Meteorol.* 92: 3-24.
- Rao K. S., Snodgrass H. F., 1981: A nonstationary nocturnal drainage flow model. *Boundary-Layer Meteorol.*, 20: 309–320.
- Reuten, C., Steyn, D. G., Strawbridge, K. B., and Bovis, P.: 2002, Air Pollutants Trapped in Slope Flow Systems, *Bull. Amer. Meteor. Soc.*, **83**, 966.
- Van Der Avoird E., Duynkerke P. G., 1999: Turbulence in a katabatic flow. Does it resemble Turbulence in stable boundary layers over flat surfaces? *Boundary-Layer Meteorol.* 92: 39-66.
- Weng W., Taylor. P.A., 2003: On modeling the one-dimensional atmospheric boundary layer. *Boundary-Layer Meteorol.* 107: 371-400.
- Whiteman C. D., 2000: Mountain meteorology: fundamentals and applications. Oxford University Press.
- Xu D., Taylor P.A., 1997: An  $\epsilon - \ell$  turbulence closure for planetary boundary-layer model: The neutrally stratified case. *Boundary-Layer Meteorol.* 84: 247–266.
- Yamada T., 1983: Simulation of nocturnal drainage flows by a  $q^2 \ell$  turbulence closure model. *J. Atmos. Sci.* 40: 91–106.